Separation and Purification Technology 354 (2025) 128733

Contents lists available at ScienceDirect

Separation and Purification Technology

journal homepage: www.elsevier.com/locate/seppur

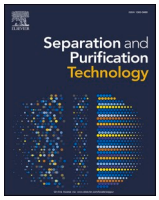

Adsorption of steroid hormone micropollutant by polyethersulfone ultrafiltration membranes with varying morphology

Han Ya Lin, Andrea I. Schäfer *

Institute for Advanced Membrane Technology (IAMT), Karlsruhe Institute of Technology (KIT), Hermann-von-Helmholtz-Platz 1, 76344 Eggenstein-Leopoldshafen, Germany

ARTICLE INFO

Keywords:
Phase inversion
Membrane support
Membrane filtration
Water treatment

ABSTRACT

The effective removal of micropollutants necessitates the use of dense membranes, such as thin-film composite (TFC) reverse osmosis (RO) and nanofiltration (NF) membranes. TFCs have a polyamide active layer interfacially polymerized on a support layer that is typically made of polysulfone (PSu) or polyethersulfone (PES). Retention by NF and RO is often incomplete because micropollutants are adsorbed to the polymer material and subsequently permeate via a combination of convection and diffusion, which evidences a breakthrough curve. When describing breakthrough phenomena, the role of the support membrane is commonly neglected, even though the adsorption in this layer can be significant. This work investigated the adsorption of steroid hormone micropollutants (17β-estradiol, E2) by fabricated and commercial PES ultrafiltration membranes with varying morphology.

By increasing the coagulation bath temperature between 10 and 70 °C, the pure water permeability increased from 13 to 3800 $L/m^2 \cdot h^{-1} \cdot bar^{-1}$, and consequently, the average pore size rose from 12 to 191 nm. The fabricated membranes with smaller pore sizes showed higher E2 removal via adsorption which can be attributed to the higher internal surface area. The adsorbed mass of fabricated PES membranes (using dimethylformamide (coded as PDG) and N-methyl-2-pyrrolidone (coded as PNG) and PES (Istanbul Technical University (ITU), with non-woven supports) varies from 0.30 to 0.60, 0.27–0.60 and 1–1.2 $ng \cdot cm^{-2}$, respectively. These values are lower than the adsorbed masses with commercial Biomax (Millipore Inc.) membranes (0.5–2.0 $ng \cdot cm^{-2}$). Ultrafiltration membranes used as support for composite membranes, nanofiltration or as filters in sample preparation benefit from lower micropollutant adsorption.

1. Introduction

Polysulfone (PSu) and polyethersulfone (PES) belong to the polysulfone family group that consists of aryl (aromatic ring), ether (–O–), and sulfone ($-SO_2-$) groups and display outstanding mechanical, thermal, and chemical stability [1,2]. These are commonly used in pressure-driven membranes as support layers of thin-film composite reverse osmosis (RO) [3] and nanofiltration (NF) [4] membranes, and separation layers in ultrafiltration (UF) [5,6] and microfiltration (MF) [7] membranes. PSu/PES polymers can be easily processed and dissolved in common organic solvents such as N-methyl-2-pyrrolidone (NMP) and dimethylformamide (DMF). These properties allow PSu/PES-based membranes to be prepared via non-solvent induced phase separation (NIPS) [8–12]. Additionally, the chemistry of PSu/PES membranes can be modified by surface coating and photo-, electron-, and thermal-induced grafting to improve the anti-fouling and separation performance [13]. Further incorporation of nanomaterials can add reactive moieties that result in reactive (adsorptive and photo-/electrocatalytic) membranes [14–17]. Among the pressure-driven membranes using PSu/PES as support, RO/NF [18] can retain small molecular weight pollutants by size exclusion and electrostatic repulsion.

RO/NF membranes are required to remove micropollutants (MPs), which typically occur at very low concentrations ($ng \cdot L^{-1}$ to $\mu g \cdot L^{-1}$) in wastewater effluents and surface waters [19,20]. Micropollutants cause health concerns (such as endocrine disrupting effects) to aquatic organisms and humans [21]. The removal of MPs with RO/NF is incomplete as the MPs pass through the RO/NF membranes by initially adsorbing to the membrane polymers and then traveling through the membrane via a combination of convection and diffusion [22–24]. Furthermore, defects formed by the poor interfacial polymerization in

* Corresponding author.
E-mail address: Andrea.Iris.Schaefer@kit.edu (A.I. Schäfer).

https://doi.org/10.1016/j.seppur.2024.128733
Received 13 May 2024; Received in revised form 28 June 2024; Accepted 5 July 2024
Available online 6 July 2024

the selective layer of RO/NF make membranes more permeable and result in lower retention for MPs [25,26]. The breakthrough phenomena are similar to those in fixed-bed reactors [27], where adsorption occurs through various interaction mechanisms of MPs with membrane polymers. Unlike in adsorptive membranes, where adsorption is favorable [28,29], in RO/NF, adsorption is unwanted [22,30,31], and hence, the characteristics of polymers and MPs need to be examined to minimize adsorption [32,33].

In general, the adsorption process of an MP onto a polymeric membrane includes three main steps: (i) transport of the MPs from the bulk solution to the external surface (or the boundary layer) of the membrane. (ii) internal mass transfer from the outer surface (or the boundary layer) of the membrane to the inner surface of the porous membrane structure, and (iii) energetic interaction between the MPs and the sites of the membrane [34]. The last step (energetic interaction), when the MPs and surface are close (~1 nm), is determined by the affinity between the MPs and surface. Neutral MPs have a high affinity for membrane polymers such as PSu/PES and polyamide (PA) via π-π interaction (if the MPs are aromatic), hydrogen bonding, van der Waals forces [35], and hydrophobic effects [24,36,37]. Negatively charged MPs can be repelled by the (negatively charged) membrane surface [38]. In contrast, neutral and especially positively charged MPs are more susceptible to adsorption by membranes, which makes removal dependent on water chemistry for some MPs [39].

In NF membranes, the adsorption of steroid hormone MPs has been examined in the thin-film polyamide layer [23,24], while PSu used as the support layer of commercial NF membranes is often neglected [24,36]. In the active layer, the pores are very small (sub-nanometers in diameter), and as a result of this close contact, the steroid hormone MPs readily partition to the polymer structure and transport in the adsorbed phase through this layer [40]. Increased pore sizes in the support structure or UF membranes result in stronger mass transfer limitations and typically lower adsorbed mass [42]. However, commercial PES (Millipore Biomax) membranes adsorb significant amounts of steroid hormones where up to 80 % removal has been reported [43,44]. Other lab-made UF PES membranes adsorbed 10–30 % of aromatic organic pollutants, including bisphenol A (BPA), ciprofloxacin, chloramphenicol, methyl orange, and methylene blue, albeit in relatively high concentrations (1 mg·L^{-1}) [45].

The combination of adsorption, intrinsic retention, and diffusion through membrane leads to the breakthrough phenomena that was observed in RO/NF and UF/MF [22,46]. Hormones gradually saturate the adsorption sites of membranes; the steroid hormones that pass through the membrane, reaching an equilibrium [22,30,31]. In RO/NF, when the membranes retain the micropollutants, the concentration polarization layer enhances diffusion and results in a steeper breakthrough curve [23]. Membrane materials that adsorb fewer micropollutants readily reach adsorption equilibrium and saturation, and a breakthrough can be observed. This can be applied in membrane fabrication using polymers with less adsorptive properties, such as hydrophilic membranes for hydrophobic micropollutants [44] and membranes with a smaller specific surface area (fewer active sites) [47–50].

In the first instance, membrane morphology will determine permeability and rejection, while porosity and flux alternate the hydraulic residence time that is required for adsorption. The support layer and UF membrane properties (pore size, porosity, and thickness) can be adjusted via the fabrication technique and configuration. Various methods for producing membranes have been proposed, including non-solvent-induced phase separation (NIPS), temperature-induced phase separation (TIPS) [53], and vapor-induced phase separation (VIPS) [54]. Among these, NIPS is commonly used in industry and laboratory fabrication [51,52]. At a given membrane thickness, membrane pore size [55–59] and porosity [60] are the morphological factors determining membrane permeability. For instance, membrane permeability increases with the decrease in polymer concentration [51,61] or the increase in coagulation bath temperature [55–59] due to increased pore size and porosity.

The surfaces of membranes fabricated via phase separation are rough and structurally heterogeneous; hence, they provide high-energy adsorption sites for MP adsorption [62,63]. Membrane pore size and porosity can be modified by controlling the concentration and molecular weight (MW) of porogens (added to form pores), such as polyethylene glycol (PEG) and polyvinylpyrrolidone (PVP) [64–69], coagulation bath temperature [56–59], and polymer concentration [51,61,71]. A lower surface area for adsorption can be attained by increasing the concentration of porogens [49]. The permeability of membranes will increase due to a larger pore size [55–59] and higher porosity [60], which is attained by decreasing the polymer concentration [51,61] or increasing coagulation bath temperature [55–59] and porogen concentration [68,72].

By casting a polymer solution on glass and immersing it in a coagulation bath (NIPS), asymmetric UF membranes can be produced with a dense layer that is sub-micrometers or several micrometers in thickness [51,52]. The finger-like or sponge-like morphology of the sub-structure can be induced by adjusting the composition of the polymer solution, pre-evaporation time, humidity, coagulation bath temperature, and composition of the coagulation bath [52,73]. Compared to cylindrical structure, the tortuosity in sponge-like structures increases the likelihood of “collision” between micropollutants and membrane polymers and enhances adsorption, while smaller pore sizes in sponge-like structures will equally enable such contact [41].

In membrane filtration, the membrane can be assumed as a plug-flow reactor [74] and the contact time (without adsorption) of adsorbate in the membrane is described with the hydraulic residence time [75]. The higher adsorption capacity was observed when the water flux was reduced, which can be attributed to the longer hydraulic residence time that allows the adsorbate to access the internal pores of materials [76,77]. To increase the hydraulic residence time, increasing membrane thickness, or reducing water flux are two methods to increase adsorption capacity [78,79].

Most studies focus on the impacts of morphology on performance concerning permeability and rejection. Although some fabrication methods for commercial membranes can be found in patents [80,81], the material properties and additives are typically proprietary information and specific details are not available to explain adsorption. In such membranes, the contribution of morphology, including pore size, surface area, macrovoids, and macrovoid-free structures, to adsorption is not well understood. This study investigates the influence of morphology, particularly the pore size and surface area, on E2 adsorption. The results of fabricated PES membranes (with macrovoid structure) are compared with the adsorption results of commercial PES membranes (with macrovoid-free structure). The specific research questions are: (i) How do the fabrication parameters (coagulation temperature and solvent) affect the pore size and surface area of PES membranes? (ii) What is the E2 adsorption of PES membranes that are fabricated with varied fabrication parameters (coagulation bath temperature and solvent type)? (iii) How does the E2 adsorption of commercial membranes (Biomax) compare with fabricated PES membranes?

2. Materials and methods

2.1. Membrane preparation and properties

The fabricated PES membranes were prepared using the NIPS method [51]. Polyethersulfone (PES, >99 %, 3100P, Solvay, Belgium), polyethylene glycol (PEG-6000, Merck, USA), dimethylformamide (DMF, >99.8 %, Sigma Aldrich, USA), and *N*-methyl-2-pyrrolidone (NMP, 99.9 %, VWR, Germany) were used in the fabrication. A mix of 14 wt% PES and 2 wt% PEG is dissolved in DMF or NMP, where 14 wt% PES was selected for the polymer concentration and 2 wt% PEG was selected to attain high membrane permeability [2,51]. The polymer solution was stirred at 50 °C for 24 h and sonicated for 10 min to remove

bubbles. The solution was then cast onto a glass plate (thickness 3.8 mm, Borofloat@33, VWR, Germany) using a doctor blade (ZAA2300, Zehntner Testing Instruments, Switzerland) with a temperature of 22 ± 2 °C and relative humidity of 44 ± 2 % maintained by an air conditioner controller (CZ-RTC4, Panasonic, Japan) and the recorded temperature and humidity were shown in Table S4. The casting height was maintained at 250 μm, and the casting rate was set to 50 mm.s^{-1}. The plate with the casted polymer solution was immersed immediately in deionized water (DI) as a non-solvent in a coagulation bath (Alpha RA24, Lauda, Germany) at different water temperatures (10–70 °C) for 5 min, then kept submerged for 12 h in a large beaker containing fresh DI water for removing residual compounds. The fabricated PES membranes are coded as PDG and PNG, where P stands for PES, D for DMF, G for PEG, and N for NMP, which are the components of membrane material. The following number refers to the coagulation bath temperature.

For reference purposes, the fabricated PES membranes (with 16 % PES and 6 % PVP, formed in a coagulation bath temperature of 25 °C coded as ITU-25 and with 16 % PES, 6 % PVP, formed in a coagulation bath temperature of 50 °C coded as ITU-50) were fabricated by MEMTEK (Istanbul Technical University, Turkey) [82]. In brief, PES (72,000 kDa, BASF, Germany) and PVP (40,000 kDa, Sigma-Aldrich, USA) were used as membrane components, and DMF (>99.8 %, Merck, Germany) was used as a solvent. The mixture of these polymers (16 % PES and 6 % PVP) was cast on a non-woven support layer (instead of glass) with a casting knife (Automatic Film Applicator, Sheen, Netherlands). The non-woven support layer introduces additional surface area for MP adsorption. The casting height was maintained at 250 μm, and the casting rate was set to 50 mm.s^{-1}. The evaporation time was set to 10 s. After evaporation, the glasses with the casted polymer solution were immersed in a coagulation bath for 5 min. The membranes were transferred to a clean container and submerged with deionized water.

The commercial PES membranes were supplied by Merck Millipore (USA) with varied molecular weight cut-offs (MWCOs), namely PBGC, PBTK, PBQK, PBHK, PBMK, and PBXK, with MWCOs of 10, 30, 50, 100, 300, and 1000 kDa, respectively. The MWCO corresponds to an average pore size of 5–62 nm [83]. The Biomax membranes have a PES-dense layer, a microporous sub-structure and a polyolefin (polyethylene and polypropylene) support layer, with a total thickness of 280 μm [84].

2.2. Characterization of membrane morphology

The cross-section membrane samples for SEM evaluation were prepared using a cryomicrotome (CM-1860UV, Leica, Germany). Before sectioning, the membrane sample was frozen in a tissue freezing medium (Leica) at −30 °C. The sample was then cut with a low-profile microtome blade (DB80LX, Leica, Germany). Scanning electron microscopy (SEM, XL 30, Philips, Netherlands) was used for Fig. 2, the SEM (Supra 60VP equipped with SE-ll detector, Zeiss, Germany) was used for Fig. 5, and the samples were coated with a 10 nm layer of conductive gold by a sputter coater (SCD005, BAL-TEC). The SEM (Ultra 55, Zeiss, Germany) was carried out for Fig. 3 and the samples were coated with a 30 nm layer of chromium using a sputter system (Z400, Leybold, Germany). A Hitachi SU8020 ultra-high resolution field emission scanning electron microscope (UHR FE- SEM) was used for Fig. 4. and the samples were sputter coated with chromium using Q150T ES coater (Quorum Technologies Ltd., Lewes, UK).

Porosity (Table S3) was measured using the weight difference between wet and dry membranes. Membrane thickness (Table S3) was measured from SEM micrographs using Image J (v 1.53k). The tool of the straight line was used for setting the scale bar. Pore size (Table S3) was calculated by both Hagen-Poiseuille [85] (water flow through the membrane with cylindrical capillaries) and Carman-Kozeny equation [86,87] (water flow through the membrane with porous medium). Membrane permeability was required to apply the above equations. The membrane permeability (Table S3) of varied membranes was measured from filtration experiments with Milli-Q water at 23 °C and varied flow rates.

To analyze the surface area of PES membranes, Nitrogen adsorption–desorption isotherms were collected at 77 K during the equilibrium interval of 30 s using an N_2 adsorption analyzer (Micromeritics, ASAP 2020). Prior to the measurement, samples were degassed at 100 °C for 6 h under vacuum. The Brunauer–Emmett–Teller (BET) method was utilized to calculate the specific surface areas using adsorption data in a relative pressure (P/P0) range from 0.02 to 0.2. The nitrogen adsorption isotherms are shown in Fig. S8.

2.3. Membrane filtration system

The filtration system, consisting of three 10 mL dead-end filtration cells (maximum pressure 5.2 bar, Millipore-8010, Germany), connected with a single peristaltic pump (Masterflex® L/S®, Cole-Parmer, USA) with a pump head (Model 07516-10, Cole-Parmer, USA), balance (AX622/E, Ohaus, USA), and a computer for data collection (see Fig. 1).

A membrane of 2.5 cm diameter (whole membrane area of 4.9 cm [2], effective membrane area of 3.8 cm^2) was fitted into the base of the membrane cell and the cell was then tightened. The filtration protocol is shown in Table S1.

In the main experiments, the pump flow rate was set to 1.2 mL.min^{-1} except for PDG-10 for all membranes. Due to the very low permeability of PDG-10, the flow rate was set to 0.3 mL.min^{-1} in this particular experiment. The stirring speed was set to 400 rpm. A total permeate mass of 180 g was collected and measured by a balance (AX622/E, Ohaus, USA). The permeate mass was converted to volume using a density of 1000 ± 10 kg.m^{-3} at 24 ± 2 °C. The temperature of the feed and pressure were recorded by temperature (TA2145, IFM, Germany) and pressure sensors (PT5415, IFM, Germany) which were connected to a data acquisition module (NI 9203, National Instruments, USA) and were monitored by LabView software (version 2014, N1, USA).

2.4. Micropollutants and solution chemistry

The steroid hormone, estradiol (E2) was chosen as a model micropollutant because it is commonly detected in surface water, outlet of wastewater effluents [88,89] and its adverse effect to aquatic organisms [90]. The stock solution was prepared from a concentrated radiolabeled solution that was supplied with a specific activity of 91 Ci·mmol^{-1}, corresponding to the specific mass activity of 1.2 • 10^4 Bq·ng^{-1}. Tritium labeled E2 (LLT, Perkin Elmer, USA) was used at a concentration of 100 ng·L^{-1} and was prepared by diluting 10 μg·L^{-1} of E2 stock solution.

100 mM NaCl (99.5 %, Thermo Scientific) and 10 mM $NaHCO_3$ (100 %, VWR) were prepared as a stock solution for the background electrolyte. Experiments were carried out in a background electrolyte of 10 mM NaCl and 1 mM $NaHCO_3$ with a neutral pH of 8.0 ± 0.1. Ultrapure Milli-Q water (Milli-Q® Reference A+, Merck) was used for preparing stock hormone solutions, stock background electrolyte solutions, and feed water.

2.5. Analysis of micropollutant concentration and water quality

A liquid scintillation counter (LSC 2500 TR/AB, Packard, USA) was used to quantify the amount of tritium (^{3}H) labeled E2 in 1 mL of permeate sample mixed with 1 mL of Ultima Gold LLT scintillation cocktail (Perkin Elmer, USA). The LSC calibration was performed by measuring the activity of tritium (Bq) in samples of known E2 concentrations. Standard solutions of E2 (0, 0.05, 0.1, 0.4, 1, 10, 50 and 100 ng·L^{-1}) were prepared by dilution of the supplied native solution. A calibration is shown in Fig. S10. A radiolabeled sample with a β-emitter, such as tritium (3H), transfers its decay energy to a scintillation cocktail, which contains an aromatic solvent and a scintillator. The majority of the decay energy from the radioactive sample is absorbed by the aromatic solvent. This solvent subsequently transfers the absorbed energy

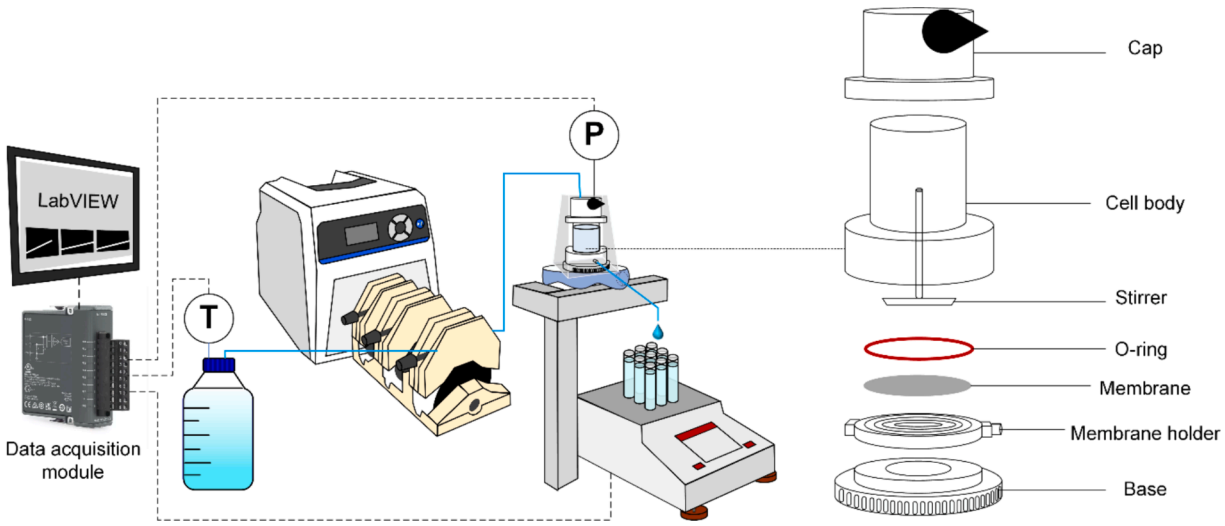

Fig. 1. Schematic of filtration process with a 10 mL Perspex stirred cell.

to the scintillator, while the scintillator emits photons of light with de-excitation. The intensity of this emitted light is measured, converted into electrical pulses and quantified to activity [91]. As a result, the concentration of radiolebelled samples can be analyzed by preparing a calibration curve using standard concentrations. The pH/conductivity meter (pH/Cond 3320, WTW, USA) with pH sensor (SenTix® 41) was used for pH measurement. The adsorbed mass (E2 adsorbed on membrane specific to membrane area) was calculated using Eq. S3 in Table S2.

The experiments of static adsorption were conducted by an incubator shaker (Innova 43, Eppendorf, Germany) at 20 ℃ and 260 rpm. Radiolabeled hormones stock solutions (10 μg/L) and non-radiolabeled hormone stock solutions (10 mg/L in methanol) were diluted with a background electrolyte solution in Milli-Q water (Merck Millipore, Germany; resistivity >18.2 MΩ/cm at 25 ℃) to obtain feed concentrations of 0.1, 1, 10, 100 and 1000 μg/L. Membrane coupons (25 mm diameter) were soaked in 100 mL of E2 solution. A sample of 2.5 mL was taken from the solution at different times (0, 0.1, 0.2, 0.5, 1, 2, 3, 4, 5, 6, 7, 24 and 26 h) to analyze E2 concentration. The adsorption isotherms are shown in Fig. S9.

3. Results and discussion

Membranes were firstly fabricated at varied parameters (coagulation bath temperature and organic solvent) and then examined for their membrane properties including cross-section, membrane permeability, average pore size, and calculated internal surface area. Secondly, E2 filtration was performed with the fabricated PES membranes to elucidate the adsorption difference caused by the coagulation bath temperature and organic solvent. Thirdly, the E2 filtration results of the fabricated PES membranes were compared with the commercial PES membranes in which the average pore size is governed by different

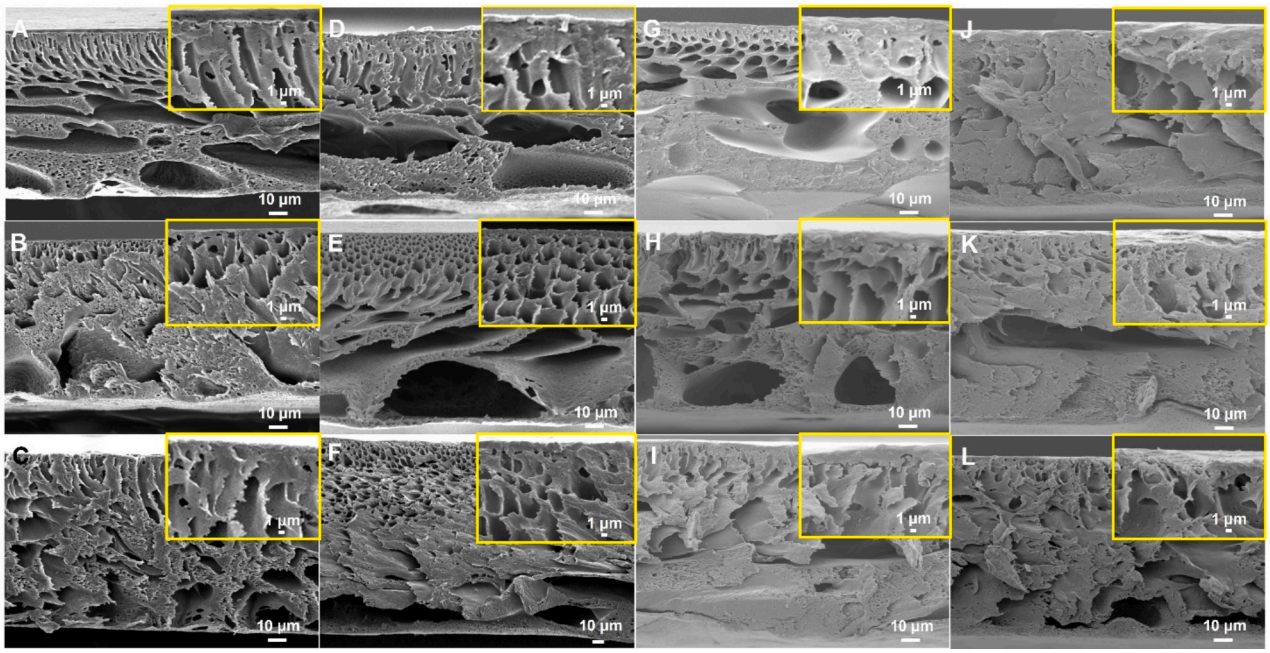

Fig. 2. Cross-section SEM images of the fabricated PES membranes with solvents DMF (PDG) and NMP (PNG) and different coagulation temperatures 10, 22, 35, 50, 60, and 70 °C (A to F for PDG and G to L for PNG), the zoom-in of the dense layer is shown in the yellow box (SEM images prepared by Tawheed Hashem (KIT-IFG)). (For interpretation of the references to colour in this figure legend, the reader is referred to the web version of this article.)

molecular weight cut-off. The pore size and internal surface area are later discussed to understand their impacts on E2 adsorption.

3.1. Membrane morphology variation with coagulation bath temperature and organic solvent

In order to understand how the coagulation temperature controls the membrane, the PES membranes were fabricated with both organic mixtures (PDG and PNG) and different coagulation bath temperature from 10 to 70 °C and visualized in SEM. The variation in pore morphology in the membrane cross-section is illustrated in Fig. 2.

A denser layer with thicknesses within 1 μm was found on top of each membrane, where separation of water components should occur. The fabricated PES membranes coagulated at higher temperatures have more macrovoids in the sub-structure below the dense layer because a higher coagulation bath temperature increases the solvent exchange rate and thus induces more macrovoids [55–59]. Additionally, the membrane thickness increased with the increase in coagulation temperature. The thickness of the PDG membranes increased from 79 to 95 μm, and that of the PNG membranes increased from 90 to 159 μm with increasing coagulation temperature from 10 to 70 °C. This trend is attributed to instantaneous de-mixing that forms porous structures, whereas slow de-mixing results in denser structures [55–57]. With the same volume of the organic mixture, the denser structure requires less membrane volume and, hence, thickness. The PNG membranes have more macrovoids and a more open sub-structure than the PDG membranes at the same coagulation temperature. This is attributed to the higher solvent exchange rate of NMP (for PNG membranes) than DMF (for PDG membranes) [58,92]. DMF induces stronger hydrogen bonding (C=O•••H–O–H) with water than NMP does when the casting solution is in contact with water in the coagulation bath, which causes gradual solidification and a lowered solvent exchange rate [92]. However, no clear differentiation between sponge and finger-like structures was obtainable. The surface morphology was visualized with SEM to reveal the variation of pore size in the dense layer with coagulation temperature (Fig. 3).

Fig. 3 (A, C) shows that the surfaces of fabricated PES membranes that have coagulated (both PNG and PDG) are grainy (where the grains are formed at 10 °C) and have small pores with a diameter of several nanometers. In contrast, the surfaces of membranes coagulated at higher temperatures (Fig. 3 (B, D)) have a more open morphology. Besides increasing the macrovoids, the higher solvent exchange rate at higher coagulation temperatures allows the broadening of pores [55–59]. At a high coagulation temperature of 70 °C, the PNG membrane shows more open surface morphology than the PDG membrane due to the faster solvent exchange rate of NMP than DMF [92].

The observations from surface and cross-section visualization are consistent, as higher coagulation temperatures result in faster solvent exchange rates and more open structures. To further confirm the influence of coagulation bath temperature on membrane morphology, alternative PES membranes (coded as ITU-25 and ITU-50) were fabricated at 25 and 50 °C in the coagulation bath. Unlike the PDG and PNG membranes, these ITU membranes were deposited on non-woven support fibers. The cross-sectional structures of the ITU membranes are shown in Fig. 4.

Fig. 4 (A, B) shows that the ITU-50 membrane (coagulation bath temperature 50 °C) has larger macrovoids with finger-like structure and a thicker cross-section than the ITU-25. Similar to the PDG and PNG series, increasing the solvent exchange rate with higher solvent coagulation bath temperatures induced larger macrovoids in ITU membranes. Comparing the ITU-25, ITU-50 with fabricated PES membranes at 22 and 50 ℃ (i.e. PDG-22, PNG-22, PDG-50 and PNG-50), the fabricated PES membranes show larger macrovoids in the sub-structure and thicker cross-section which can be attributed to fast diffusion of non-solvent to the polymer-rich solution and no non-woven support as a barrier for the water intrusion [73].

For various fabricated membranes (PDG, PNG, and ITU series) a higher coagulation bath temperature consistently results in more macrovoids in the substructure and a thicker cross-section. The larger the pore sizes and the more open sub-structure (due to coagulation bath temperature), the higher the water permeability observed for all membrane types (PDG, PNG, and ITU) (Figs. S1 and S2). The more open structure results in larger mass transfer limitations (through the bulk and boundary layer) for adsorption and a potentially reduced surface area.

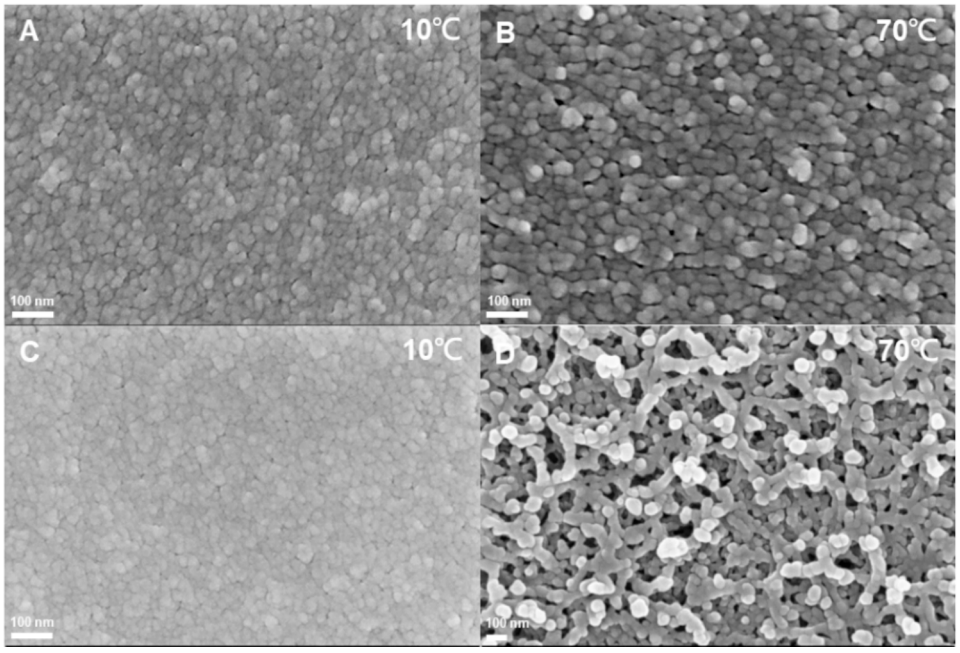

Fig. 3. Surface SEM images of the fabricated PES membranes, (A, B) PDG and (C, D) PNG, coagulated at 10 and 70 °C (SEM images provided by Kristina Fischer (IOM, Leipzig)).

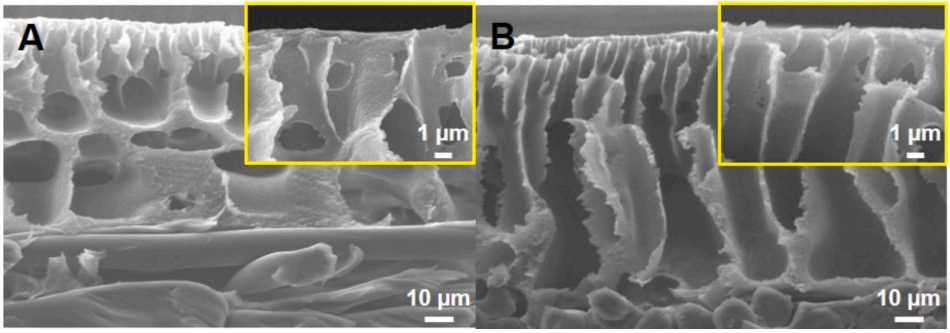

Fig. 4. Cross-section SEM images of (A) ITU-25 and (B) ITU-50, the zoomed images of the dense layers are shown in the yellow box (SEM images provided by Prof. Joanna Grzechulska-Damszel (West Pomeranian University of Technology in Szczecin). (For interpretation of the references to colour in this figure legend, the reader is referred to the web version of this article.)

3.2. Membrane morphology of commercial PES membrane (Biomax)

The morphology of commercial PES membranes (Biomax) was examined for reference purposes, as these membranes show consistent separation results from literature [93,94] and good availability of morphological data (MWCO, pore size, thickness, and membrane materials) [84]. The cross-section images of Biomax membranes (various MWCO) are shown in Fig. 5.

Fig. 5 shows a microporous sub-structure underneath a thin, dense layer (the thickness of this dense layer was not accurately quantified in the SEM but was in the order of 1 μm). Unlike in fabricated membranes, the finger-like macrovoids are not present in these commercial membranes, as the sub-structure appears relatively homogeneous with uniform micropore sizes (in the order of 0.1–1 μm). The dense sub-structure allows more surface area for adsorption, while smaller pore/macrovoid size reduce mass transfer limitations. In the case of membrane thickness (including a thin, dense layer and microporous sub-structure), 300 and 1000 kDa have the thickest cross-sections with a number of 102 and 93 μm, respectively. 10, 30, 50, and 100 kDa are in the range of 50–66 μm.

Steroid hormone (E2) adsorption will be examined in breakthrough experiments at the same flux (190 $L{\cdot}m^{-2}{\cdot}h^{-1}$) to determine how varying membrane morphology affects adsorption.

3.3. Breakthrough curves of estradiol

To determine how the varied membrane morphology (more open morphology was attained with PNG compared with PDG and at higher coagulation bath temperatures) impacts micropollutant adsorption, the breakthrough curves that indicate how E2 concentrations varied with permeate volume are shown in Fig. 6.

Fig. 6 (A, B) shows the E2 concentration increased gradually due to adsorption to reach the feed concentration of 100 $ng{\cdot}L^{-1}$ after collecting 100 mL of permeate. From 100 to 180 mL, the permeate concentration was equal to the feed concentration. This confirms that the membranes did not reject E2, as expected, given the small size of the E2 molecule. When the permeate concentration is equal to the feed concentration, adsorption saturation occurs, which means the adsorbed mass reaches a maximum and does not further increase with increasing permeate volume. Fig. 6 (C, D) shows the adsorbed mass decreased from 0.6 to 0.3 $ng{\cdot}cm^{-2}$ with increasing coagulation bath temperature (from 10 to 70 °C) with both PDG and PNG membrane series.

The PDG and PNG membranes showed similar adsorbed mass at the same coagulation bath, although the sub-structure of the PNG membranes is more open than that of the PDG membranes. The fabricated ITU membranes were then examined to determine whether the decrease in adsorbed mass with increasing coagulation temperature could be confirmed. The results are shown in Fig. 7.

Fig. 7A shows ITU-25 and ITU-50 reached 100 $ng{\cdot}L^{-1}$ after collecting 180 mL of permeate, which shows membrane adsorption saturation. Fig. 7B shows that ITU-50 coagulated at higher temperatures has lower adsorbed mass than ITU-25. ITU-50 reached a constant 1 $ng{\cdot}cm^{-2}$ of adsorbed mass after collecting 180 mL of permeate, while the adsorbed mass of ITU-25 was 1.3 $ng{\cdot}cm^{-2}$ at 180 mL and still appeared to increase further.

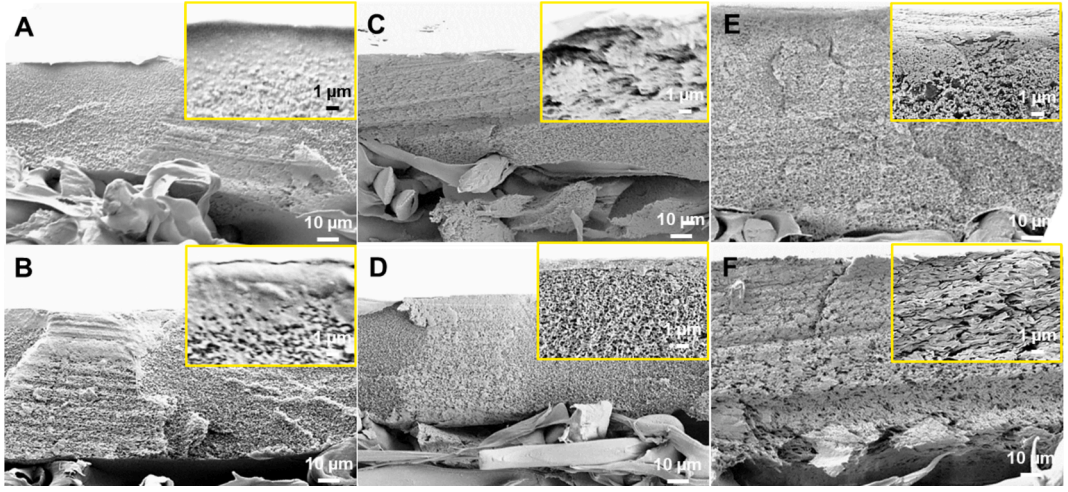

Fig. 5. Cross-section SEM images of the Biomax membranes (the non-woven supports are excluded). 10, 30, 50, 100, 300, and 1000 kDa (A to F) and zoomed images of dense layers (thickness is not quantifiable) and microporous substructures are shown in the yellow box (SEM images provided by Dr. Justine Nyarige (IMT, KIT)). (For interpretation of the references to colour in this figure legend, the reader is referred to the web version of this article.)

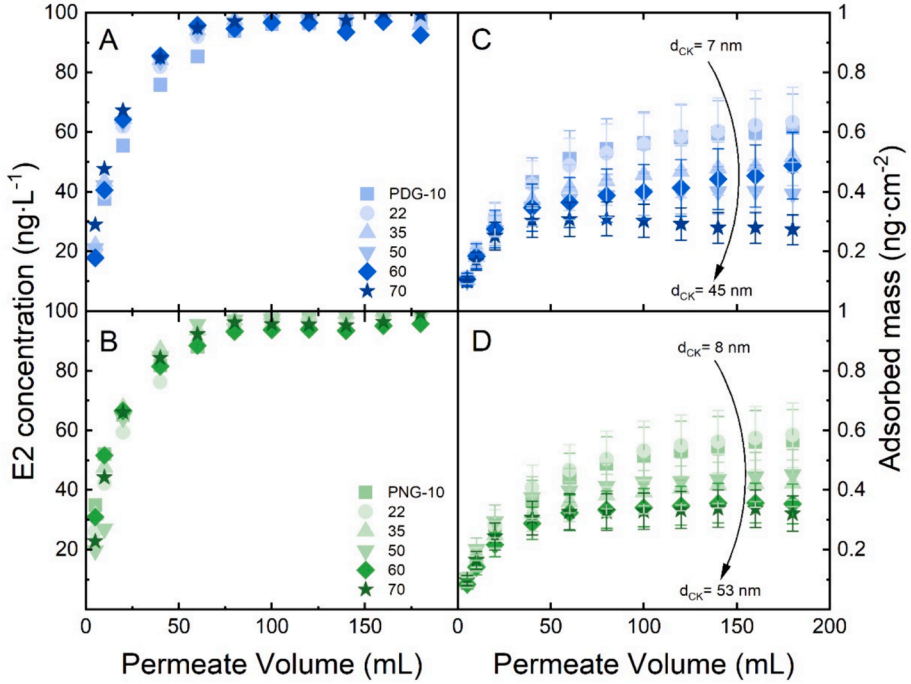

Fig. 6. (A, B) E2 concentration and (C, D) adsorbed mass as functions of permeate volume of PDG and PNG membranes (E2 100 ng·L^{-1}, pH 8.1 ± 0.1, 22.6 ± 0.4 ℃, 1.2 mL·min^{-1} for all membranes and 0.3 mL·min^{-1} for PDG-10), d_{CK}: pore size using Carman-Kozeny equation, the fabricated PES membranes are coded as PDG and PNG, where P stands for PES, D for DMF, G for PEG, and N for NMP, which are the components of membrane material, the subsequent number refers to the coagulation bath temperature.

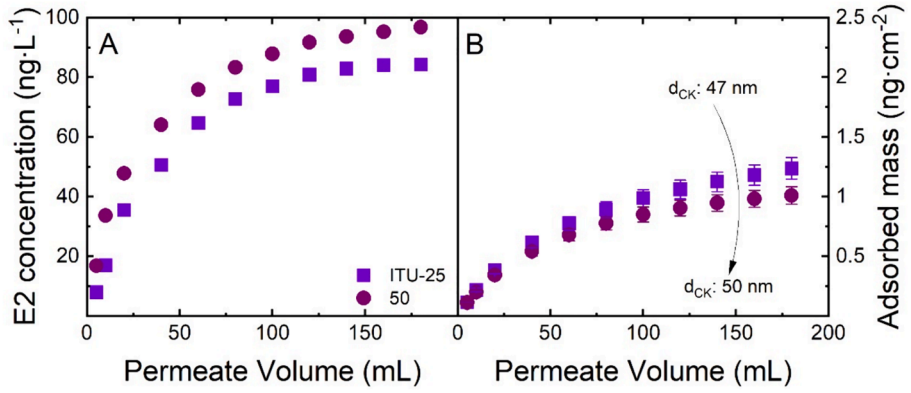

Fig. 7. (A) E2 concentration and (B) adsorbed mass as functions of permeate volume of ITU membranes (E2 100 ng·L^{-1}, pH 8.1 ± 0.1, 22.6 ± 0.4 ℃, 1.2 mL·min^{-1}), d_{CK}: pore size using Carman-Kozeny equation.

The adsorbed mass by PES membranes (ITU) was higher (1 ng·cm^{-2} at 50 °C and 1.3 ng·cm^{-2} at 25 °C) than PDG and PNG membranes (0.4 ng·cm^{-2} at 50 °C and 0.6 ng·cm^{-2} at 22 °C). The difference between these membranes may be attributed to the higher surface area (it is noted that the ITU membrane also comprises a non-woven support that provides adsorption sites) and higher PES content in the membranes (14 % for PDG and PNG and 16 % for ITU), allowing the dense layer to have a higher density [48,66] and additional adsorption sites for E2 [51,61].

In the next section, the adsorbed mass will be examined with commercial PES membranes (Biomax) as a reference to the adsorbed mass with fabricated PES membranes (PDG, PNG, and ITU). This approach was chosen as the role of the pore size cannot be elucidated in the fabricated PES membranes as several morphology parameters are changed simultaneously in fabrication.

3.4. Estradiol breakthrough curve of biomax membrane

Biomax membranes have sponge-like, macrovoid-free structures and are available over a broad MWCO range (pore size from 9 to 36 nm). The E2 adsorption of Biomax membranes for a range of membrane MWCO from 10 to 1000 kDa (Fig. 8) can be compared to the more heterogeneous fabricated PES membranes that contain macrovoids.

In Fig. 8A, the higher MWCO membranes (300 and 1000 kDa) reached 100 ng.L^{-1} of feed concentration after collecting 100 mL of permeate volume and displayed a steeper breakthrough than the lower MWCO membranes (10–100 kDa). Fig. 8B shows the adsorbed mass decreases with increasing MWCO; 10 to 100 kDa adsorbed about 2 ng·cm^{-2}, and 300 and 1000 kDa achieved adsorption saturation of 0.7 and 0.5 ng·cm^{-2}, respectively. This can be attributed to the reduction in pore size where surface area increases and mass transfer limitation in the dense layer reduces with decreasing pore size.

After understanding the difference in breakthrough curves and

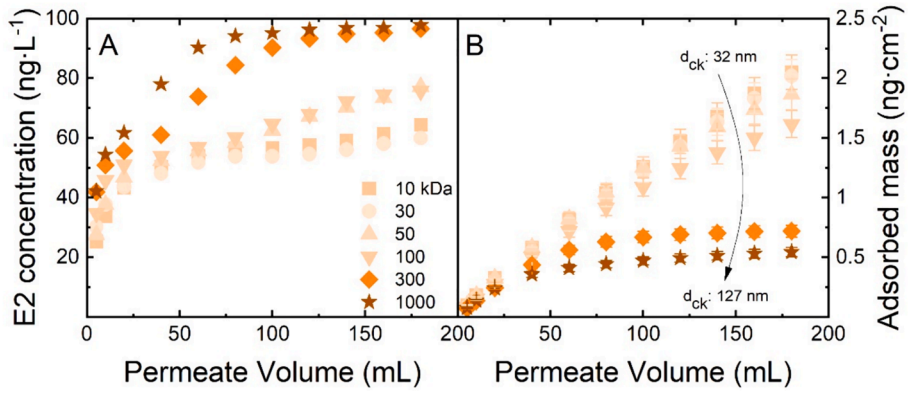

Fig. 8. (A) E2 concentration and (B) adsorbed mass as functions of permeate volume of Biomax® membranes (E2 100 ng·L^{-1}, pH 8.1 ± 0.1, 22.6 ± 0.4 ℃, 1.2 mL·min^{-1}), d_{CK}: pore size using Carman-Kozeny equation.

adsorbed mass caused by the varied membrane morphology, the influence of hydraulic residence time on E2 adsorption is then investigated since it is controlled by membrane thickness and porosity.

3.5. Hydraulic residence time of fabricated PES and commercial membranes

The hydraulic residence time determines the contact time of E2 in the membranes without adsorption, and it increases with thicker cross-section and higher membrane porosity. To elucidate if the hydraulic residence time enhances the E2 adsorption in the fabricated membranes that coagulated at higher bath temperatures. The membrane porosity, membrane thickness and calculated hydraulic residence time are shown in Table S3. The adsorbed mass with hydraulic residence time is shown in Fig. 9.

Fig. 9 shows that adsorbed mass decreases with hydraulic residence time, which is surprising. The hydraulic residence time of the fabricated PES membrane (PDG, PNG and ITU) increases slightly with coagulation bath temperature, which was attributed to the increase of both membrane thickness and porosity. However, the adsorbed mass of the fabricated PES membrane (PDG, PNG and ITU) does not show a positive increment with hydraulic residence time. In the case of Biomax membranes, the higher MWCO membranes (300 and 1000 kDa) have a higher hydraulic residence time than the lower MWCO membranes (10, 30, 50, 100 and 300 kDa). Nevertheless, the adsorbed mass is lower, suggesting the hydraulic residence time is not a limiting factor for E2 adsorption in both fabricated PES and commercial membranes. The lower adsorption may be attributed to the lower surface areas [64,72] and stronger mass transfer limitations [95] with decreasing pore size. It is challenging to control membrane morphology in a systematic manner, one parameter at a time.

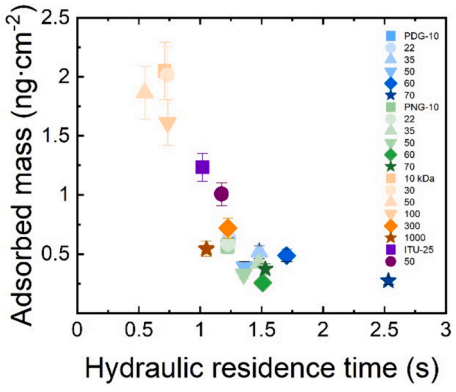

Fig. 9. Adsorbed mass as functions of the hydraulic residence time of PES membranes (E2 100 ng·L^{-1}, pH 8.1 ± 0.1, 22.6 ± 0.4 ℃, 1.2 mL·min^{-1}).

Findings from PES-fabricated (PDG, PNG, and ITU) and commercial membranes suggest that pore size or membrane internal surface area plays an important role, which will be illuminated in more detail.

3.6. Effect of average pore size and internal surface area on E2 adsorption

The adsorbed mass is illustrated in Fig. 10A to elucidate the effect of average pore size on E2 adsorption. Since the fabricated PES membranes have asymmetric structures, the calculated pore size represented the 'average' pore size in the membrane. This clearly compromises the results. The average pore size was calculated using the Carman-Kozeny equations (Eq. S11 in Table S2). The shape of the pore was assumed to be a cylinder shape for calculating surface area from the surface-to-volume ratio, and the calculated results are shown in Table S3. The calculated averaged pore size does not present the real pore size on the surface but is used for understanding the influence of pore size on E2 adsorption. It is noted that by averaging the pore size, the effect of mass transfer (which is more limiting in the sub-structure macrovoids than in the skin layer pores) is excluded in the adsorption analysis. The adsorbed mass expressed in the mass of the membrane is shown in Figure S6.

Fig. 10A shows the fabricated PES membranes (PDG, PNG) with a smaller average pore size have higher E2 adsorption. This can be attributed to the denser skin layer [51,61,71] and reduced diffusion time (Eq. S12) for adsorption. This effect has been characterized in membrane chromatography [96]. However, in asymmetric membranes, the mass transfer is more efficient, and hence adsorption is stronger in the dense layer than in the sub-structure macrovoids. In the case of PES (ITU) membranes, it has a bigger average pore size (70–150 nm) than PES (PDG, PNG), and higher E2 adsorption. This may be due to the higher mass of porogen that induced a bigger pore size, while the higher E2 adsorption could be due to the higher PES content in membranes, which provides extra active sites for adsorption [51,61,71]. In the case of Biomax membranes, membranes adsorb 2 to 3 times more E2 (1.5–2 ng·cm^{-2}) than macrovoid membranes (PNG, PDG, and PES (ITU)). It is anticipated that this is due to the macrovoid-free structure of Biomax membranes. The average pore size and internal surface of membranes are typically modified simultaneously. It is important to consider the internal surface area to elucidate the contribution of both morphological parameters. The cross-section of Biomax membranes has a macrovoid-free structure, which is different from fabricated PES and PES (ITU). Here, the internal surface areas were calculated to investigate its impact on E2 adsorption. The shape of the pore was assumed to be cylindrical, and the internal surface area (Eq. S9) was estimated from the surface-to-volume ratio and volume of PES in the membrane coupon (see Table S3).

Fig. 10B shows that the calculated internal surface area decreased with increasing coagulation bath temperature in fabricated PES membranes (PNG and PDG). This is because the change in coagulation bath

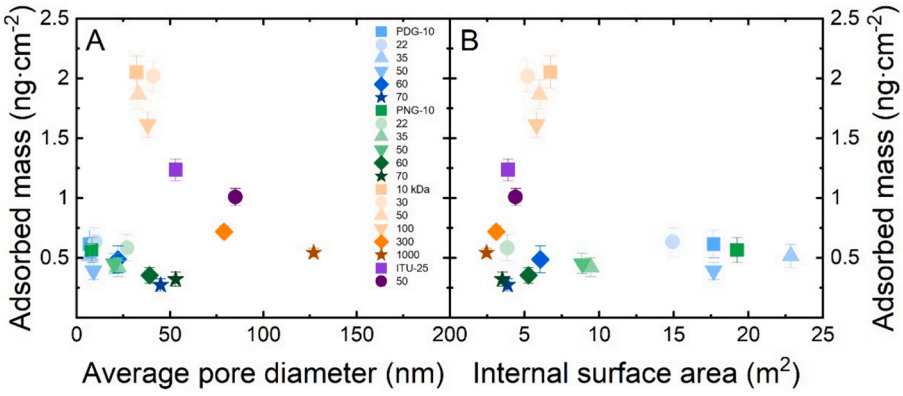

Fig. 10. Adsorbed mass as functions of average pore size and internal surface area of PES membranes (E2 100 ng·L^{-1}, pH 8.1 ± 0.1, 22.6 ± 0.4 ℃, 1.2 mL·min^{-1}).

temperature reduces the number of pores in membranes while increasing the diameter of pores [70]. However, the increase in surface area does not influence E2 adsorption for PDG, PNG and PES (ITU) membranes. In the case of Biomax membranes, it shows the adsorbed mass increased with increasing internal surface area which can be attributed to the additional active sites for E2 adsorption. Further analysis of specific surface area was conducted by gas adsorption analyzer. Fig. S7 shows a similar trend that the increase in specific surface area does not have an obvious impact on E2 adsorption in the fabricated PES membranes (PDG and PNG) but shows a positive increment in the Biomax membranes. Furthermore, Biomax membranes have sponge-like structures with a tortuosity of 1.8 to 2.5, which is higher than a finger-like structure [97,98]. The sponge-like structure can cause better contact between the E2 and the membrane polymer (tortuosity and friction) and hence enhance adsorbed mass [41].

4. Conclusions

This research attempts to investigate how the membrane morphology is affected by the fabrication parameters and how these parameters control the E2 adsorption by comparing the commercial PES membranes in filtration. This challenging objective seeing that it is not possible to selectively alter specific morphology parameters.

From the SEM images and membrane permeability, the coagulation bath temperature created bigger pores and porous structures in the membrane. A larger pore size was obtained from the membranes fabricated with NMP.

The fabricated PES (PDG, PNG) and PES (ITU) membranes that have a smaller average pore size have higher E2 adsorption (0.6 and 1.3 ng·cm^{-2}, respectively). This can be attributed to the denser skin layer and decreasing pore size, which have less mass transfer limitation in E2 adsorption. The internal surface area is affected by membrane porosity, shape of pores, tortuosity, pore size, and membrane thickness, which makes it difficult to conclude how surface area affects E2 adsorption. However, the sponge-like (macrovoid-free) structure of Biomax can contribute to higher friction between E2 and membrane polymer than the finger-like macrovoid structure and cause higher E2 adsorption.

The findings demonstrate that by controlling the membrane fabrication parameters, the adsorption of MPs can be reduced during filtration. The adsorbed mass (0.2–0.6 ng·cm^{-2}) are lower than the adsorbed masses with Biomax membranes (0.5–2.0 ng·cm^{-2}). Lower adorption is beneficial for the use of membranes in composites, as support layers in thin-film composite membranes as well as in filters in the analysis of steroid hormone micropollutants.

CRediT authorship contribution statement

Han Ya Lin: Writing – original draft, Visualization, Validation, Methodology, Investigation, Formal analysis, Data curation. **Andrea I. Schäfer:** Writing – review & editing, Supervision, Resources, Project administration, Methodology, Funding acquisition, Conceptualization.

Declaration of competing interest

The authors declare that they have no known competing financial interests or personal relationships that could have appeared to influence the work reported in this paper.

Acknowledgments

Helmholtz Association for Recruitment Initiative for IAMT funding. BMBF RealMethod for project funding (No.01DR20011). Collaboration partner of RealMethod from Japan (Hokkaido University), France (Université de Poitiers), and Turkey (Istanbul Technical University, ITU). Millipore for providing Biomax membrane (PB series). Dr. Kristina Fischer (IOM, Leipzig) for SEM images of membrane surface (Fig. 3). Dr. Tawheed Hashem (KIT-IFG) for SEM images of the PDG and PNG membranes (Fig. 2). Prof. Joanna Grzechulska-Damszel (West Pomeranian University of Technology in Szczecin, Poland) for SEM images of PES (ITU) (Fig. 4). Dr. Justine Nyarige (KIT-IMT) for SEM images of Biomax membranes (Fig. 5). Dr. Chhabilal Regmi for membrane fabrication (fabricated PES series). Zhi-Fu Lin (IAES and IPHD, National Tsing Hua University) for providing gas adsorption analysis. Rabia Ardıç and Mehmet Emin Pasaglaşaoğlu (ITU, Turkey) for membrane provision (PES(ITU) series) and critical discussion about membrane fabrication, respectively. Dr. Siqi Liu and Dr. Minh N. Nguyen (KIT-IAMT) provided the 3D figure of E2 and revised the manuscript, respectively. Prof. Sylwia Mozia (West Pomeranian University of Technology) provided thorough comments on the manuscript.

Appendix A. Supplementary data

Filtration protocol. Determination of membrane permeability. Filtration data (pressure, mass, temperature and water flux). Data analysis for filtration performance and membrane properties. Determination of membrane pore size and surface area. Record of membrane environmental data. Effect of average pore size and internal surface area on E2 adsorption. Calibration curve of LSC. Error analysis. Supplementary data to this article can be found online at https://doi.org/10.1016/j.seppur.2024.128733.

References

[1] S. Lee, E.Y. Choi, C.K. Kim, Fabrication and properties of nanofiltration membranes assembled with chitosan on poly(ether sulfone) membranes surface-functionalized with acyl chloride groups, Ind. Eng. Chem. Res. 58 (16) (2019) 6679–6686.

[2] H. Mokarizadeh, S. Moayedfard, M.S. Maleh, S.I.G.P. Mohamed, S. Nejati, M. R. Esfahani, The role of support layer properties on the fabrication and performance of thin-film composite membranes: The significance of selective layer-support layer connectivity, Sep. Purif. Technol. 278 (2021) 119451.

[3] A.O. Rashed, A.M.K. Esawi, A.R. Ramadan, Novel polysulfone/carbon nanotube-polyamide thin film nanocomposite membranes with improved water flux for forward osmosis desalination, ACS Omega 5 (24) (2020) 14427–14436.

[4] A. Marjani, A.T. Nakhjiri, M. Adimi, H.F. Jirandehi, S. Shirazian, Effect of graphene oxide on modifying polyethersulfone membrane performance and its application in wastewater treatment, Sci. Rep. 10 (1) (2020) 2049.

[5] P. Kallem, Y. Ibrahim, S.W. Hasan, P.L. Show, F. Banat, Fabrication of novel polyethersulfone (PES) hybrid ultrafiltration membranes with superior permeability and antifouling properties using environmentally friendly sulfonated functionalized polydopamine nanofillers, Sep. Purif. Technol. 261 (2021) 118311.

[6] Y.J. Jo, E.Y. Choi, N.W. Choi, C.K. Kim, Antibacterial and hydrophilic characteristics of poly(ether sulfone) composite membranes containing zinc oxide nanoparticles grafted with hydrophilic polymers, Ind. Eng. Chem. Res. 55 (28) (2016) 7801–7809.

[7] K.H. Yun, K. Sharma, H.U. Kim, T.-H. Bae, Modification of a PES microfiltration membrane to enhance sterile filtration by inhibiting protein adsorption, J. Ind. Eng. Chem. 123 (2023) 311–319.

[8] F. Russo, F. Galiano, F. Pedace, F. Aricò, A. Figoli, Dimethyl isosorbide as a green solvent for sustainable ultrafiltration and microfiltration membrane preparation, ACS Sustain. Chem. Eng. 8 (1) (2020) 659–668.

[9] D. Lou, Z. Hou, H. Yang, Y. Liu, T. Wang, Antifouling membranes prepared from polyethersulfone grafted with poly(ethylene glycol) methacrylate by radiation-induced copolymerization in homogeneous solution, ACS Omega 5 (42) (2020) 27094–27102.

[10] M.A.A. Shahmirzadi, S.S. Hosseini, G. Ruan, N. Tan, Tailoring PES nanofiltration membranes through systematic investigations of prominent design, fabrication and operational parameters, RSC Adv. 5 (61) (2015) 49080–49097.

[11] S. Mazinani, S. Darvishmanesh, A. Ehsanzadeh, B. Van der Bruggen, Phase separation analysis of Extem/solvent/non-solvent systems and relation with membrane morphology, J. Membr. Sci. 526 (2017) 301–314.

[12] M. He, S. Zhang, Y. Su, R. Zhang, Y. Liu, Z. Jiang, Manipulating membrane surface porosity and pore size by in-situ assembly of Pluronic F127 and tannin, J. Membr. Sci. 556 (2018) 285–292.

[13] C. Zhao, J. Xue, F. Ran, S. Sun, Modification of polyethersulfone membranes – a review of methods, Prog. Mater Sci. 58 (1) (2013) 76–150.

[14] G. Kaminska, J. Bohdziewicz, J.I. Calvo, P. Prádanos, L. Palacio, A. Hernández, Fabrication and characterization of polyethersulfone nanocomposite membranes for the removal of endocrine disrupting micropollutants from wastewater, Mechanisms and Performance. *J. Membr. Sci.* 493 (2015) 66–79.

[15] K. Fischer, A. Gawel, D. Rosen, M. Krause, A. Abdul Latif, J. Griebel, A. Prager, A. Schulze, Low-temperature synthesis of anatase/rutile/brookite TiO2 nanoparticles on a polymer membrane for photocatalysis, Catalysts 7 (7) (2017) 209.

[16] S. Ma, F. Yang, X. Chen, C.M. Khor, B. Jung, A. Iddya, G. Sant, D. Jassby, Removal of As(III) by electrically conducting ultrafiltration membranes, Water Res. 204 (2021) 117592.

[17] K. Fischer, P. Schulz, I. Atanasov, A. Abdul Latif, I. Thomas, M. Kühnert, A. Prager, J. Griebel, A. Schulze, Synthesis of high crystalline TiO2 nanoparticles on a polymer membrane to degrade pollutants from water, Catalysts 8 (9) (2018) 376.

[18] J. Heo, S. Kim, N. Her, C.M. Park, M. Yu, Y. Yoon, Chapter 5 - Removal of contaminants of emerging concern by FO, RO, and UF membranes in water and wastewater, in: A.J. Hernández-Maldonado, L. Blaney (Eds.), Contaminants of Emerging Concern in Water and Wastewater, Butterworth-Heinemann, 2020; pp 139-176.

[19] Y. Yang, X. Zhang, J. Jiang, J. Han, W. Li, X. Li, K.M. Yee Leung, S.A. Snyder, P.J. J. Alvarez, Which micropollutants in water environments deserve more attention globally? Environ. Sci. Technol. 56 (1) (2022) 13–29.

[20] R.P. Schwarzenbach, B.I. Escher, K. Fenner, T.B. Hofstetter, C.A. Johnson, U. Von Gunten, B. Wehrli, The challenge of micropollutants in aquatic systems, Science 313 (5790) (2006) 1072–1077.

[21] P. Bhatt, G. Bhandari, M. Bilal, Occurrence, toxicity impacts and mitigation of emerging micropollutants in the aquatic environments: Recent tendencies and perspectives, J. Environ. Chem. Eng. 10 (3) (2022) 107598.

[22] L.D. Nghiem, A.I. Schäfer, Adsorption and transport of trace contaminant estrone in NF/RO membranes, Environ. Eng. Sci. 19 (6) (2002) 441–451. Acccessed 2023/06/03.

[23] A. Imbrogno, A.I. Schäfer, Micropollutants breakthrough curve phenomena in nanofiltration: Impact of operational parameters, Sep. Purif. Technol. 267 (2021) 118406.

[24] A.J.C. Semião, A.I. Schäfer, Removal of adsorbing estrogenic micropollutants by nanofiltration membranes. Part A—Experimental evidence, J. Membr. Sci. 431 (2013) 244–256.

[25] A. Ben-David, R. Bernstein, Y. Oren, S. Belfer, C. Dosoretz, V. Freger, Facile surface modification of nanofiltration membranes to target the removal of endocrine-disrupting compounds, J. Membr. Sci. 357 (1) (2010) 152–159.

[26] X. Song, B. Gan, S. Qi, H. Guo, C.Y. Tang, Y. Zhou, C. Gao, Intrinsic nanoscale structure of thin film composite polyamide membranes: Connectivity, defects, and structure–property correlation, Environ. Sci. Technol. 54 (6) (2020) 3559–3569.

[27] K.H. Chu, Breakthrough curve analysis by simplistic models of fixed bed adsorption: In defense of the century-old Bohart-Adams model, Chem. Eng. J. 380 (2020) 122513.

[28] Y. Wu, N. Zhang, G. Yuen, C.-F. de Lannoy, Cross-linked iron nanoparticle-doped reduced graphene oxide membranes for micropollutant removal from water, Chem. Eng. J. 455 (2023) 140624.

[29] Z. Liao, M.N. Nguyen, G. Wan, J. Xie, L. Ni, J. Qi, J. Li, A.I. Schäfer, Low pressure operated ultrafiltration membrane with integration of hollow mesoporous carbon nanospheres for effective removal of micropollutants, J. Hazard. Mater. 397 (2020) 122779.

[30] J. Wolters, M. Tagliavini, A.I. Schäfer, Removal of steroid hormone micropollutants by UF-PBSAC composite in presence of organic matter, J. Membr. Sci. 592 (2019) 117315.

[31] M. Askari, B. Rezaei, A. Mousavi Shoushtari, M. Abdouss, Performance improvements in structural characteristics of chitosan-based nanofibrous composite membrane for using in liquid filtration, J. Taiwan Inst. Chem. Eng. 56 (2015) 77–83.

[32] A.I. Schäfer, I. Akanyeti, A.J.C. Semião, Micropollutant sorption to membrane polymers: a review of mechanisms for estrogens, Adv. Colloid Interface Sci. 164 (1) (2011) 100–117.

[33] Z. Jia, J. Pan, C. Tian, D. Yuan, Twisted molecule-based hyper-crosslinked porous polymers for rapid and efficient removal of organic micropollutants from water, RSC Adv. 8 (64) (2018) 36812–36818.

[34] S. Hao, Z. Jia, J. Wen, S. Li, W. Peng, R. Huang, X. Xu, Progress in adsorptive membranes for separation – a review, Sep. Purif. Technol. 255 (2021) 117772.

[35] Y.-L. Liu, K. Xiao, A.-Q. Zhang, X.-M. Wang, H.-W. Yang, X. Huang, Y.F. Xie, Exploring the interactions of organic micropollutants with polyamide nanofiltration membranes: a molecular docking study, J. Membr. Sci. 577 (2019) 285–293.

[36] Y.-L. Liu, X.-M. Wang, H.-W. Yang, Y.F. Xie, Adsorption of pharmaceuticals onto isolated polyamide active layer of NF/RO membranes, Chemosphere 200 (2018) 36–47.

[37] K. Kimura, G. Amy, J. Drewes, Y. Watanabe, Adsorption of hydrophobic compounds onto NF/RO membranes: an artifact leading to overestimation of rejection, J. Membr. Sci. 221 (1) (2003) 89–101.

[38] Y.-L. Liu, X.-M. Wang, H.-W. Yang, Y.F. Xie, Quantifying the influence of solute-membrane interactions on adsorption and rejection of pharmaceuticals by NF/RO membranes, J. Membr. Sci. 551 (2018) 37–46.

[39] Z. Zhu, P. Wu, G. Liu, X. He, B. Qi, G. Zeng, W. Wang, Y. Sun, F. Cui, Ultrahigh adsorption capacity of anionic dyes with sharp selectivity through the cationic charged hybrid nanofibrous membranes, Chem. Eng. J. 313 (2017) 957–966.

[40] A.J.C. Semião, A.I. Schäfer, Estrogenic micropollutant adsorption dynamics onto nanofiltration membranes, J. Membr. Sci. 381 (1) (2011) 132–141.

[41] M.N. Nguyen, M.L. Jue, S.F. Buchsbaum, S.J. Park, F. Vollnhals, S. Christiansen, F. Fornasiero, A.I. Schäfer, Interplay of the forces governing steroid hormone micropollutant adsorption in vertically-aligned carbon nanotube membrane nanopores, Nat. Commun. 15 (1) (2024) 1114.

[42] E. Worch, Modelling the solute transport under nonequilibrium conditions on the basis of mass transfer equations, J. Contam. Hydrol. 68 (1) (2004) 97–120.

[43] J. Zhang, M.N. Nguyen, Y. Li, C. Yang, A.I. Schäfer, Steroid hormone micropollutant removal from water with activated carbon fiber-ultrafiltration composite membranes, J. Hazard. Mater. 391 (2020) 122020.

[44] D. Jermann, W. Pronk, M. Boller, A.I. Schäfer, The role of NOM fouling for the retention of estradiol and ibuprofen during ultrafiltration, J. Membr. Sci. 329 (1) (2009) 75–84.

[45] H.-C. Zhang, S.-X. Gao, G.-P. Sheng, Immobiling enzyme-like ligand in the ultrafiltration membrane to remove the micropollutant for the ultrafast water purification, J. Membr. Sci. 636 (2021) 119566.

[46] L.D. Nghiem, A.I. Schäfer, M. Elimelech, Removal of natural hormones by nanofiltration membranes: measurement, modeling, and mechanisms, Environ. Sci. Technol. 38 (6) (2004) 1888–1896.

[47] M. Ulbricht, W. Ansorge, I. Danielzik, M. König, O. Schuster, Fouling in microfiltration of wine: the influence of the membrane polymer on adsorption of polyphenols and polysaccharides, Sep. Purif. Technol. 68 (3) (2009) 335–342.

[48] Z. Li, X. Luo, Y. Li, Reed rhizome residue-based activated carbon adsorption ultrafiltration membranes for enhanced MB removal, ACS Omega 7 (48) (2022) 43829–43838.

[49] D. Cartalade, A. Vernhet, Polar Interactions in flavan-3-ol adsorption on solid surfaces, J. Agric. Food Chem. 54 (8) (2006) 3086–3094.

[50] A.K. Shukla, J. Alam, M. Alhoshan, L.A. Dass, M.R. Muthumareeswaran, Development of a nanocomposite ultrafiltration membrane based on polyphenylsulfone blended with graphene oxide, Sci. Rep. 7 (1) (2017) 41976.

[51] N. Evenepoel, S. Wen, M. Tilahun Tsehaye, B. Van der Bruggen, Potential of DMSO as greener solvent for PES ultra- and nanofiltration membrane preparation, J. Appl. Polym. Sci. 135 (28) (2018) 46494.

[52] G.R. Guillen, Y. Pan, M. Li, E.M.V. Hoek, Preparation and characterization of membranes formed by nonsolvent induced phase separation: a review, Ind. Eng. Chem. Res. 50 (7) (2011) 3798–3817.

[53] Y. Tang, Y. Lin, W. Ma, X. Wang, A review on microporous polyvinylidene fluoride membranes fabricated via thermally induced phase separation for MF/UF application, J. Membr. Sci. 639 (2021) 119759.

[54] N. Ismail, A. Venault, J.-P. Mikkola, D. Bouyer, E. Drioli, T.H. Kiadeh, N., Investigating the potential of membranes formed by the vapor induced phase separation process, J. Membr. Sci. 597 (2020) 117601.
[55] J. Xu, Y. Tang, Y. Wang, B. Shan, L. Yu, C. Gao, Effect of coagulation bath conditions on the morphology and performance of PSf membrane blended with a capsaicin-mimic copolymer, J. Membr. Sci. 455 (2014) 121–130.
[56] M. Esmaeili, J. Lahti, T. Virtanen, M. Mänttäri, M. Kallioinen, The interplay role of vanillin, water, and coagulation bath temperature on formation of antifouling polyethersulfone (PES) membranes: application in wood extract treatment, Sep. Purif. Technol. 235 (2020) 116225.
[57] E. Saljoughi, M. Amirilargani, T. Mohammadi, Effect of PEG additive and coagulation bath temperature on the morphology, permeability and thermal/chemical stability of asymmetric CA membranes, Desalination 262 (1) (2010) 72–78.
[58] Y.L. Thuyavan, N. Anantharaman, G. Arthanareeswaran, A.F. Ismail, Impact of solvents and process conditions on the formation of polyethersulfone membranes and its fouling behavior in lake water filtration, J. Chem. Technol. Biotechnol. 91 (10) (2016) 2568–2581.
[59] J. Li, G. Chen, S. Luo, H. Pang, C. Gao, S. Huang, S. Liu, S. Qin, Tuning the microstructure of SMA/CPVC membrane for enhanced separation performance by adjusting the coagulation bath temperature, J. Appl. Polym. Sci. 139 (20) (2022) 52148.
[60] D.Y. Koseoglu-Imer, The determination of performances of polysulfone (PS) ultrafiltration membranes fabricated at different evaporation temperatures for the pretreatment of textile wastewater, Desalination 316 (2013) 110–119.
[61] H.H. Wang, J.T. Jung, J.F. Kim, S. Kim, E. Drioli, Y.M. Lee, A novel green solvent alternative for polymeric membrane preparation via nonsolvent-induced phase separation (NIPS), J. Membr. Sci. 574 (2019) 44–54.
[62] Z. Wang, X. Luo, Z. Song, K. Lu, S. Zhu, Y. Yang, Y. Zhang, W. Fang, J. Jin, Microporous polymer adsorptive membranes with high processing capacity for molecular separation, Nat. Commun. 13 (1) (2022) 4169.
[63] W. Su-Hua, D. Bing-zhi, H. Yu, Adsorption of bisphenol A by polysulphone membrane, Desalination 253 (1) (2010) 22–29.
[64] X. Fang, J. Li, X. Li, X. Sun, J. Shen, W. Han, L. Wang, Polyethyleneimine, an effective additive for polyethersulfone ultrafiltration membrane with enhanced permeability and selectivity, J. Membr. Sci. 476 (2015) 216–223.
[65] A. Idris, N. Mat Zain, M.Y. Noordin, Synthesis, characterization and performance of asymmetric polyethersulfone (PES) ultrafiltration membranes with polyethylene glycol of different molecular weights as additives, Desalination 207 (1) (2007) 324–339.
[66] B. Vatsha, J.C. Ngila, R.M. Moutloali, Preparation of antifouling polyvinylpyrrolidone (PVP 40K) modified polyethersulfone (PES) ultrafiltration (UF) membrane for water purification, Phys. Chem. Earth, Parts a/b/c 67–69 (2014) 125–131.
[67] Y.-C. Lin, H.-H. Tseng, D.K. Wang, Uncovering the effects of PEG porogen molecular weight and concentration on ultrafiltration membrane properties and protein purification performance, J. Membr. Sci. 618 (2021) 118729.
[68] C. Kahrs, J. Schwellenbach, Membrane formation via non-solvent induced phase separation using sustainable solvents: a comparative study, Polymer 186 (2020) 122071.
[69] B. Chakrabarty, A.K. Ghoshal, M.K. Purkait, Effect of molecular weight of PEG on membrane morphology and transport properties, J. Membr. Sci. 309 (1) (2008) 209–221.
[70] P. Fang, S. Cui, Z. Song, L. Zhu, M. Du, C. Yang, Phase-field simulation of the effect of coagulation bath temperature on the structure and properties of polyvinylidene fluoride microporous membranes prepared by a nonsolvent-induced phase separation, ACS Omega 8 (1) (2023) 180–189.
[71] G.R. Guillen, G.Z. Ramon, H.P. Kavehpour, R.B. Kaner, E.M.V. Hoek, Direct microscopic observation of membrane formation by nonsolvent induced phase separation, J. Membr. Sci. 431 (2013) 212–220.
[72] J.-Y. Zhou, Y. Shen, M.-J. Yin, Z.-P. Wang, N. Wang, Z. Qin, Q.-F. An, Polysulfate membrane prepared with a novel porogen for enhanced ultrafiltration performance, Chem. Eng. J. Adv. 12 (2022) 100397.
[73] H. Wu, H. Zhao, Y. Lin, X. Liu, H. Yao, L. Yu, H. Wang, X. Wang, Fabrication of polysulfone membrane with sponge-like structure by using different non-woven fabrics, Sep. Purif. Technol. 297 (2022) 121553.
[74] O. Levenspiel, Chemical Reaction Engineering, John wiley & sons, 1998.
[75] B. Qiu, S. Fan, Y. Wang, J. Chen, Z. Xiao, Y. Wang, Y. Chen, J. Liu, Y. Qin, S. Jian, Catalytic membrane micro-reactor with nano ZIF-8 immobilized in membrane pores for enhanced Knoevenagel reaction of Benzaldehyde and Ethyl cyanoacetate, Chem. Eng. J. 400 (2020) 125910.
[76] J. Tejedor, R. Álvarez-Briceño, V.H. Guerrero, C.A. Villamar-Ayala, Removal of caffeine using agro-industrial residues in fixed-bed columns: Improving the adsorption capacity and efficiency by selecting adequate physical and operational parameters, J. Water Process Eng. 53 (2023) 103778.
[77] V. Diniz, S. Rath, Adsorption of aqueous phase contaminants of emerging concern by activated carbon: Comparative fixed-bed column study and in situ regeneration methods, J. Hazard. Mater. 459 (2023) 132197.
[78] Z. Wang, S. Guo, B. Zhang, J. Fang, L. Zhu, Interfacially crosslinked β-cyclodextrin polymer composite porous membranes for fast removal of organic micropollutants from water by flow-through adsorption, J. Hazard. Mater. 384 (2020) 121187.
[79] P.B. Trinh, A.I. Schäfer, Removal of glyphosate (GLY) and aminomethylphosphonic acid (AMPA) by ultrafiltration with permeate-side polymer-based spherical activated carbon (UF–PBSAC), Water Res. 250 (2024) 121021.
[80] W.K. Gabriel Tkacik, N. Satav, P. Goddard, Ultrafiltration membranes and methods of making United States US10118133B2, 2018.
[81] A.E. Allegrezza, Jr., Burke, Edmund T. Composite ultrafiltration membranes, EP0245863B1, 1992.
[82] M.E. Pasaoglu, S. Guclu, I. Koyuncu, Polyethersulfone/polyacrylonitrile blended ultrafiltration membranes: preparation, morphology and filtration properties, Water Sci. Technol. 74 (3) (2016) 738–748.
[83] E. Worch, Eine neue Gleichung zur Berechnung von Diffusionskoeffizienten gelöster Stoffe, 1993.
[84] Merck Millipore, Ultrafiltration membranes for macromolecule processing. Merck Millipore, 2024. https://www.lenntech.com/Data-sheets/Millipore-Ultrafiltration-Membranes-L.pdf (Accessed 01.02.2024).
[85] A.K. Pabby, S.S. Rizvi, A.M.S. Requena, Handbook of membrane separations: chemical, pharmaceutical, food, and biotechnological applications, CRC Press, 2008.
[86] B. Kruczek, Carman–Kozeny equation, in: E. Drioli, L. Giorno (Eds.), Encyclopedia of Membranes, Springer, 2015, pp 306-308.
[87] A. Lee, J.W. Elam, S.B. Darling, Membrane materials for water purification: design, development, and application, Environ. Sci. Water Res. Technol. 2 (1) (2016) 17–42.
[88] C. He, Z. Yin, J. He, J. Lv, C. Wang, Occurrence and photodegradation of typical steroid hormones in surface water of urban lakes in Wuhan, China, J. Environ. Chem. Eng. 10 (6) (2022) 108602.
[89] M. Durcik, A. Grobin, R. Roškar, J. Trontelj, L. Peterlin Mašič, Estrogenic potency of endocrine disrupting chemicals and their mixtures detected in environmental waters and wastewaters, Chemosphere 330 (2023) 138712.
[90] J.O. Ojoghoro, M.D. Scrimshaw, J.P. Sumpter, Steroid hormones in the aquatic environment, Sci. Total Environ. 792 (2021) 148306.
[91] M.F. L'Annunziata, A. Tarancón, H. Bagán, J.F. García, Chapter 6 - Liquid scintillation analysis: principles and practice, in: M.F. L'Annunziata (Ed.), Handbook of Radioactivity Analysis (Fourth Edition), Academic Press, 2020, pp 575–801.
[92] S. Alibakhshi, M. Youssefi, S.S. Hosseini, A. Zadhoush, Significance of thermodynamics and rheological characteristics of dope solutions on the morphological evolution of polyethersulfone ultrafiltration membranes, Polym. Eng. Sci. 61 (3) (2021) 742–753.
[93] A.L. Zydney, Protein separations using membrane filtration: New opportunities for whey fractionation, Int. Dairy J. 8 (3) (1998) 243–250.
[94] D.B. Burns, A.L. Zydney, Contributions to electrostatic interactions on protein transport in membrane systems, AIChE J 47 (5) (2001) 1101–1114.
[95] C. Boi, Membrane adsorbers as purification tools for monoclonal antibody purification, J. Chromatogr. B 848 (1) (2007) 19–27.
[96] J. Chen, B. Yu, H. Cong, Y. Shen, Recent development and application of membrane chromatography, Anal. Bioanal. Chem. 415 (1) (2023) 45–65.
[97] W.A. Phillip, M. Amendt, B. O'Neill, L. Chen, M.A. Hillmyer, E.L. Cussler, Diffusion and flow across nanoporous polydicyclopentadiene-based membranes, ACS Appl. Mater. Interfaces 1 (2) (2009) 472–480.
[98] Y. Tang, J. Xu, C. Gao, Ultrafiltration membranes with ultrafast water transport tuned via different substrates, Chem. Eng. J. 303 (2016) 322–330.